LAWRENCE
LIVERMORE
NATIONAL
LABORATORY

LLNL-JRNL-848862

Comparative Analysis of Sublimation and Thermal Decomposition of TATB

B. Koroglu, A. Burnham, I. Mashiana, C. Arose, J. Crowhurst, J. Reynolds

May 8, 2023

propellants explosives pyrotechnics

Disclaimer

LLNL-JRNL-848862

Propellants, Explosives, Pyrotechnics

Full Paper

Comparative Analysis of Sublimation and Thermal Decomposition of TATB

Batikan Koroglu[a]*, Alan K. Burnham[a], [b], Imren Mashiana, Ana Racoveanu[a], Christopher Arose[a], Jonathan C. Crowhurst[a], John G. Reynolds[a]

Abstract: This experimental study investigated the effects of confinement, starting mass, and heating rate on TATB thermal decomposition and sublimation using a combined Thermo-Gravimetric Analyzer and Differential Scanning Calorimetry (TGA/DSC) instrument. The confinement of volatile products was varied using different pinhole sizes with TGA/DSC pans. The measurements showed the open pan experiments without lids/pinholes resulted in complete sublimation of TATB between 320°C and 360°C. The heat of sublimation was determined to be 176 kJ/mol, consistent with literature data obtained from other experimental techniques. The use of pinholes suppressed the sublimation of TATB such that the decrease in pinhole size resulted in 1) an increase in the enthalpy of reaction and an increase in the amount of carbonaceous material remaining at the end of decomposition, and 2) convergence of the two peak temperatures corresponding to maximum heat flow and maximum weight loss. Also, a transition from a two-exotherm thermal decomposition behavior towards a single-exotherm occurred as the pinhole size was decreased for a given starting mass or as the starting mass was increased for a given pinhole size. These results indicate the kinetics of TATB sublimation, TATB thermal decomposition, and gas diffusion out of a TGA/DSC pan can all compete and result in significantly different enthalpies, amounts of remaining materials, and peak temperatures depending on the pinhole size and starting mass used in the measurements. The results also indicate precise control of process variables (pinhole size, starting mass, and heating rate) in TGA/DSC measurements is required for thermal safety assessment of explosives.

Keywords: TATB, thermal decomposition kinetics, sublimation, diffusion, DSC, TGA

1 Introduction

TATB (1,3,5-triamino-2,4,6-trinitro benzene) is a prototypical insensitive energetic molecule. Understanding the origin and extent of insensitivity of TATB is important for developing models to predict its behavior in abnormal thermal environments. Koroglu et al. recently reported a detailed review of the literature on the thermal decomposition chemistry of TATB[1]. They also utilized the kinetic effect of isotopic substitution to help elucidate the TATB decomposition pathways. TATB underwent sublimation before thermal decomposition, requiring a crucible with a small pinhole to minimize material loss due to sublimation. However, the effects of pinhole size on sublimation and thermal decomposition kinetics were not explored. Burnham et al. investigated differential scanning calorimetry (DSC) measurements as a function of gas pressure for a given pinhole size[2]. The DSC measurements showed a transition from a two-exotherm behavior towards a single exotherm and a substantial increase in the enthalpy of thermal decomposition when the gas pressure was increased from 0.1 MPa to 7 MPa. These recent works suggest conducting a systematic study to explore the effects of experimental variables (e.g., pinhole size, starting mass, and ramp rate) on thermal decomposition/sublimation kinetics of TATB.

Few studies have investigated the effects of pinhole (or orifice) size on thermal decomposition and sublimation behaviors of energetic materials. The uses of open and closed DSC pans were shown to result in a transition from endothermic evaporation to exothermic decomposition for 2,4,6-trinitrotoluene (TNT), 1,3,3-Trinitroazetidine (TNAZ), and ammonium perchlorate (AP)[3–5]. For a given pinhole size, a similar transition in DSC curves was observed for 3,5-dinitro-1H-pyrazole (35-DNP) when the environmental pressure was increased from 0.1 MPa to 5 MPa[6]. Behrens showed even a 0.5-mm-diameter orifice resulted in complete evaporation of 3-amino-5-nitro-l,2,4-triazole (ANTA) inside the high vacuum environment of a simultaneous thermogravimetric modulated beam mass spectrometer[7]. Therefore, the orifice size was reduced to 0.025 mm to observe the decomposition products. These studies indicate the right combination of pinhole size and external pressure is required to suppress sublimation so that reliable thermal decomposition data can be obtained. For example, a study on TATB thermal decomposition reported a relatively low E_a value[8] compared to the other studies[2,9–11], and later studies[12] attributed this discrepancy to the domination of sublimation.

The choice of pinhole size seems to be somewhat arbitrary in thermal analysis of energetic materials as long as the evaporation/sublimation is suppressed. However, the level of confinement of volatiles can influence the thermal decomposition kinetics of high explosives.

[a] Lawrence Livermore National Laboratory, 7000 East Avenue, Livermore, CA, 94550
[b] M.H. Chew and Associates, 7633 Southfront Road Ste 170, Livermore, CA 94551
* Corresponding author email: koroglu1@llnl.gov

For example, decreasing the pinhole size (e.g., 0.100 mm, 0.025 mm, and 0.005 mm) was shown to increase the rate of thermal decomposition for various explosives (e.g., HMX, RDX)[7,13–15]. This was attributed to enhanced autocatalysis with increased level of gaseous products containment. The confinement of volatiles was also studied using five different orifice sizes between 0.010 and 1 mm to help develop a decomposition mechanism for triamino-guanidinium 5,5-azobitetrazolate (TAGzT)[16]. Larger orifices reduced the number of secondary reactions, allowing the first steps of decomposition to be explored, whereas small orifices were used to promote secondary reactions between the decomposition products. To the best of our knowledge, there is no study on the effect of pinhole size on TATB thermal decomposition kinetics, mechanism, or sublimation.

Although there is not a specific experimental recipe in terms of pinhole size, starting mass, and heating rate for thermal analysis of energetic materials that go through sublimation, previous DSC studies investigated the effect of pinhole size on vapor pressure measurements of various other substances[17–22]. These past studies helped establish the ASTM E1782-22 method[23], which recommends pinhole sizes between 0.050 to 0.075 mm with 40-µL-volume pans for vapor pressure measurements at atmospheric pressures using 1 to 5 mg of solid (or 1 to 5 µL of liquid) at a heating rate of 5 °C/min. Increasingly larger pinholes (e.g., 0.350 mm) are recommended for vapor pressure measurements at lower external pressures (e.g., 0.2 kPa), because 0.050 to 0.075-mm pinholes lead to self-pressurization inside the DSC pan when the measurements are performed below atmospheric pressures. The self-pressurization effect shifts the boiling point to higher temperatures and broadens the endothermic peak and thus lowers the accuracy of the onset temperature (i.e., boiling point) analysis. Although these studies are particularly important for vapor pressure measurements, they also shed light on the influence of pinhole size on sublimation/evaporation endotherms measured by DSC.

In this study, we investigate the effects of pinhole size, starting mass, and heating rate on TATB thermal decomposition and sublimation. The results of this study will guide acquisition and interpretation of thermal analysis data on TATB. In addition, the measured data will be useful for developing models to study the interplay between gas advection, gas diffusion, thermal decomposition, and sublimation/evaporation kinetics.

2 Experimental Section

2.1 Combined Thermo-Gravimetric Analyzer (TGA) and Differential Scanning Calorimeter (DSC) Measurements

A new TGA/DSC system (Mettler Toledo, TGA/DSC3+) was used for the experiments. All tests were performed at atmospheric pressure with 100 mL/min of N_2 gas flow (split 80:20 between furnace and balance). The vendor calibrated instrument was first tested with well-known materials to verify the accuracy of the weight and heat flow measurements. The accuracy of the weight signal was checked using calcium oxalate monohydrate (purity > 99%), which decomposes in three steps:

$CaC_2O_4•H_2O\ (s) \rightarrow CaC_2O_4\ (s) + H_2O\ (g)$
$CaC_2O_4\ (s) \rightarrow CaCO_3\ (s) + CO\ (g)$
$CaCO_3\ (s) \rightarrow CaO\ (s) + CO_2\ (g)$

Figure 1 shows the measured weight signal as a function of temperature during thermal decomposition of calcium oxalate monohydrate as it was heated up to 1000 °C in an alumina pan. Measured percentages of weight losses due to H_2O and CO_2 differ from theoretical values only by 0.1% for the first and third reactions, respectively. The second step shows a slightly higher discrepancy (0.5%), which can be attributed to the formation of CO_2 in the presence of CO according to the Boudouard equilibrium reaction: $2CO \leftrightarrow CO_2\ (g) + C\ (s)$[24]. We confirmed the presence of CO_2 in the second step of the decomposition process by transferring the product gases into a Mass Spectrometer (Pfeiffer, Thermo-Star GSD320).

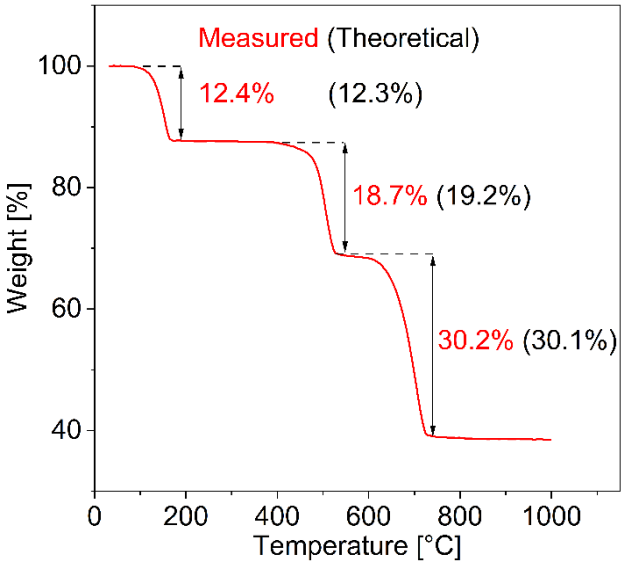

Figure 1. The weight loss percentages of calcium oxalate monohydrate measured by TGA.

The mass spectrometry measurements also revealed it took 30 min to purge the TGA/DSC system with N_2 to eliminate O_2, which was introduced through air when the system was opened during sample placement. Preliminary measurements performed without prior N_2 purging showed big differences between measured and theoretical weight losses for the second step of $CaC_2O_4•H_2O(s)$ decomposition. This should be due to the exothermic reaction between CO and O_2 ($2CO + O_2 \rightarrow 2CO_2$). The DSC measurements also confirmed the presence of the exothermic step without prior N_2 purging. Therefore, the measurements shown in Figure 1 and all the subsequent tests were performed with an hour-long N_2 gas purge at room temperature before heating the samples.

The accuracy of heat flow measurements was checked by heating Zn (Metter Toledo, purity: 99.995%) and Pb (Trace Sciences International, purity 98.9%) in separate experiments. These two elements were chosen because the sublimation and thermal decomposition temperatures of TATB lie in between the melting points of Pb (327.5°C) and Zn (419.5°C). Figure 2 displays the

DSC curves. The measured melting points of Pb and Zn differ from their previously reported values[25] by 0.1°C and 0.2°C, whereas the enthalpies differ by 6% and 5%, respectively.

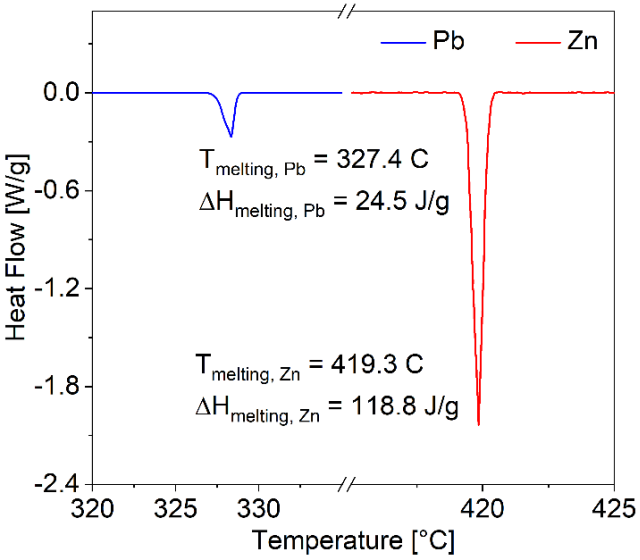

Figure 2. Melting temperatures and enthalpies of Pb and Zn measured by DSC.

2.2 Samples

TATB used in this work has a purity of 98% as measured by high performance liquid chromatography[26]. Pressed samples of TATB were used in this study. The pressed sample was cut into small pieces and a single piece was used for each experiment. The single piece of TATB was weighed before the experiments using a 0.1-µg resolution micro-balance (*Mettler Toledo, XPR6 U*). The sample was placed inside an aluminum crucible of 40-µL volume. A press was used to hermetically seal an aluminum lid on to the crucible. The lid was either purchased from the vendor pre-drilled (0.050-mm and 0.075-mm) or pierced to make a pinhole.

2.3. Experimental Conditions

Table 1 summarizes the experimental conditions for the TATB experiments. The measured data (e.g., enthalpy, remaining mass, etc.) are also included in the table, but they will be discussed in the results section. The pinhole size, starting mass, and heating rate can all influence the self-heating of samples. Self-heating results in large temperature gradients across the sample and therefore should be avoided for thermal analysis. The three variables (pinhole size, starting mass, and heating rate rate) were chosen such that the maximum heat flow (HF) signal did not exceed 8 mW, which is the ASTM limit for self-heating[23]. A few data points that slightly exceeded the 8-mW limit were also included in the results section to demonstrate the self-heating effect.

Table 1: Summary of experimental conditions (heating rate, pinhole size, and starting mass) and measured data (peak heat flow, specific enthalpy, percentage of remaining material, and temperatures at peak heat flow and peak weight loss rate)

Test No	Heating rate [°C/min]	Pinhole size [mm]	Starting mass [mg]	Peak Heat Flow [mW]	Specific Enthalpy [mJ/mg]	Percentage of remaining mass [%]	Temperature at peak heat flow [°C]	Temperature at peak weight loss rate [°C]
1	10	6.0 (open)	0.223	-1.15	-681	0.0	343.3	340.7
2		0.75	0.203	0.06	-326	5.9	385.2	381.6
3		0.35	0.218	1.09	269	8.6	385.8	384.9
4		0.075	0.194	5.93	1134	15.9	384.3	384.9
5		0.050	0.195	6.42	1238	25.4	383.6	384.2
6		(closed)	0.179	6.21	1442	27.6	384.6	385.1
7		0.075	0.120	2.72	990	20.3	386.3	386.0
8			0.136	3.78	1170	20.1	385.5	385.5
9			0.145	4.37	1448	22.4	386.0	385.8
10			0.182	5.65	1337	16.6	385.5	385.7
11			0.203	8.47	1365	21.1	383.7	384.4
12			0.222	8.35	1578	21.9	384.3	384.9
13	5		0.186	1.09	222	21.2	375.4	374.8
14			0.217	1.72	669	22.5	375.3	374.7
15			0.228	2.38	860	21.6	375.3	375.0
16			0.248	4.03	1225	24.2	374.8	374.6
17			0.262	4.55	1273	26.7	374.6	374.5
18			0.314	6.29	1338	25.9	374.1	374.2
19			0.337	4.19	957	22.7	374.4	374.5
20			0.366	4.79	1136	22.8	374.8	374.7
21			0.378	8.82	1332	24.5	373.4	373.6
22			0.408	8.24	1514	25.2	373.9	374.1
23		0.75	0.259	0.10	-306	9.8	373.5	368.8

24	0.300	0.29	-157	10.2	373.9	370.4
25	0.368	0.34	25	11.2	374.4	371.0
26	0.402	0.52	28	11.5	374.8	372.1
27	0.485	1.57	307	16.1	374.5	372.9
28	0.554	2.77	483	16.6	373.7	373.2
29	0.612	4.64	566	19.5	373.5	373.6
30	0.698	4.73	660	18.1	374.3	374.1
31	0.774	9.71	785	19.5	373.4	373.6

Four different pinhole sizes, an open pan (i.e., without a lid), and a closed pan (sealed lid without a pinhole) were used to investigate the effect of confinement for a given starting mass (nominally 0.2 mg of TATB). The 0.050-mm and 0.075-mm pinholes were laser drilled by Mettler Toledo and TA Instruments, respectively. The 0.350-mm and 0.750-mm pinholes were prepared in-house. The heating rate was set to 10 °C/min for these experiments (Tests 1 to 6 in Table 1). The influence of starting mass was explored for two different pinhole sizes (0.075 mm and 0.75 mm) and two different heating rates (10°C/min and 5 °C/min). The starting mass was varied between 0.120 mg and 0.222 mg for the measurements performed using a 0.075 mm pinhole at 10 °C/min (Tests 7 to 12 in Table 1). The heating rate was decreased to 5 °C/min in subsequent experiments, enabling us to explore a wider range of starting mass without self-heating (HF < 8 mW)[23]. The starting mass ranged from 0.186 mg to 0.408 mg with 0.075-mm pinholes (Tests 13 to 22 in Table 1), whereas it varied between 0.259 mg and 0.774 mg with 0.75-mm pinholes (Tests 23 to 31 in Table 1). For all experiments, the sample heating ended at 500 °C.

Figure 3 (a) displays a picture of one of the aluminum pans used for the experiments with a vendor-provided pinhole of nominal diameter 0.0750 mm. Figure 3 (b) shows a magnified image of the pinhole. Image-J program[27] was used to convert the image to a binary image as shown in Figure 3(c) to detect the edges of the pinhole and to determine the orifice area. The corresponding average diameter was determined to be 0.0768 mm. The same procedure was applied for the other pans/lids used in this study, and a 12% difference at most was observed between the measured pinhole size and the nominal values reported by the vendor. The difference between the measured pinhole size and nominal values reported in this study was at most 5% for the pinholes prepared in-house (0.35-mm and 0.75-mm pinholes).

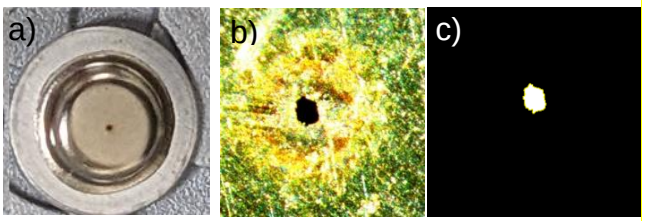

Figure 3. (a) Picture of a nominally 0.0750-mm pinhole lid. (b) Optical microscope image of the pinhole. (c) Processed image in black and white with a yellow contour drawn around the hole. The pinhole size was determined to be 0.0768 mm.

3. RESULTS

Figure 4 shows an example TGA/DSC measurement of TATB. Heat flow (red curve), weight loss (blue curve), and rate of weight loss (green curve) are plotted as a function of temperature. The enthalpy, remaining mass, and peak temperatures were determined from similar measurements and tabulated in Table 1. A 0.05-mm pinhole was used for the result shown in Figure 4 (Test No 5 in Table 1). The gas-phase products accounted for 74.6% of the starting weight, whereas 25.4% of the weight remained as black char at the end of the test at 500 °C. The enthalpy of thermal decomposition was determined to be 1237.6 J/g, which was calculated by integrating the heat flow curve over time. The time limits of integration corresponded to 300 °C and 400 °C.

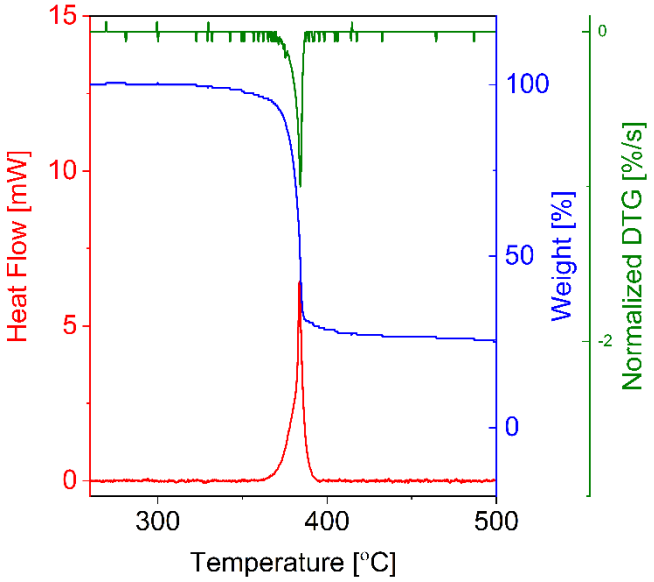

Figure 4. Heat flow (red curve), weight loss (blue), and normalized rate of weight loss (green) as a function of sample temperature; 0.050 mm pinhole lid; 10 °C/min heating rate.

Figure 4 shows the rate of weight loss has a single peak, whereas the exotherm has a leading shoulder during TATB decomposition. The peak temperatures corresponding to maximum rate of weight loss (384.2 °C) and maximum heat flow (383.6 °C) were different by 0.6 °C only. Some of the past studies reported two exotherms[28,29] and a single weight loss curve[30], whereas others[31] reported a single exotherm similar to that depicted in Figure 4. As discussed in the next section, the pinhole size, starting mass, and ramp rate influence the shape and relative intensities of the heat flow curves and the temperature differences between the peak heat flow and peak rate of weight loss.

3.1. Effect of Confinement

Figure 5 (a) compares the DSC curves obtained from experiments performed with six different pinhole sizes. A broad endotherm was observed from 320 °C to 360 °C for the experiment performed without a lid (i.e., open pan). This means TATB entirely sublimed in the open-pan test. As the orifice size was decreased to 0.75 mm and 0.35 mm, two exotherms became apparent. Further decrease of the orifice size to 0.075 mm and 0.050 mm suppressed sublimation and resulted in a transition from two exothermic peaks towards a single peak. An experiment performed without a perforated lid (i.e., nominally closed) resulted in a very similar DSC curve. The weight signal still decreased during this test (not shown), indicating the aluminum crucible leaked due to pressure build-up inside the pan.

Figure 5 (b) shows the enthalpy of reaction as a function of pinhole size. Note that the nominally closed pan was assigned a pinhole size of 0.001 mm. The enthalpy increased with decreasing pinhole size because sublimation became less significant. The enthalpy determined from the open pan test result is 681 J/g (42 kcal/mol), which is very close to the heat of sublimation measured by Langmuir (40 kcal/mol)[32] and Knudsen (43 kcal/mol)[33] effusion experiments performed under vacuum pressures (e.g., 10^{-6} Torr).

Figure 5 (c) shows the amount of remaining material at the end of the thermal decomposition tests as a function of pinhole size. Due to complete sublimation, there was not any material left when the experiments were performed in an open pan. As the pinhole size decreased, the weight loss leveled out at around 25%. Figure 5 (d) shows the peak temperatures corresponding to the maximum heat flow (T_{HF}) and maximum rate of weight loss (T_{DTG}). The two temperatures were different from each other by 4°C when there was significant sublimation (e.g., open pan and 0.75 mm pinhole tests). The difference ($T_{HF} - T_{DTG}$) decreased to 1.8°C and 0.6°C as the pinhole size was decreased to 0.35 mm and 0.075 mm, respectively. Figure 5 (d) also shows an increase in the peak temperatures as the pinhole size was decreased (i.e., a transition occurs from a sublimation-dominated regime towards thermal decomposition).

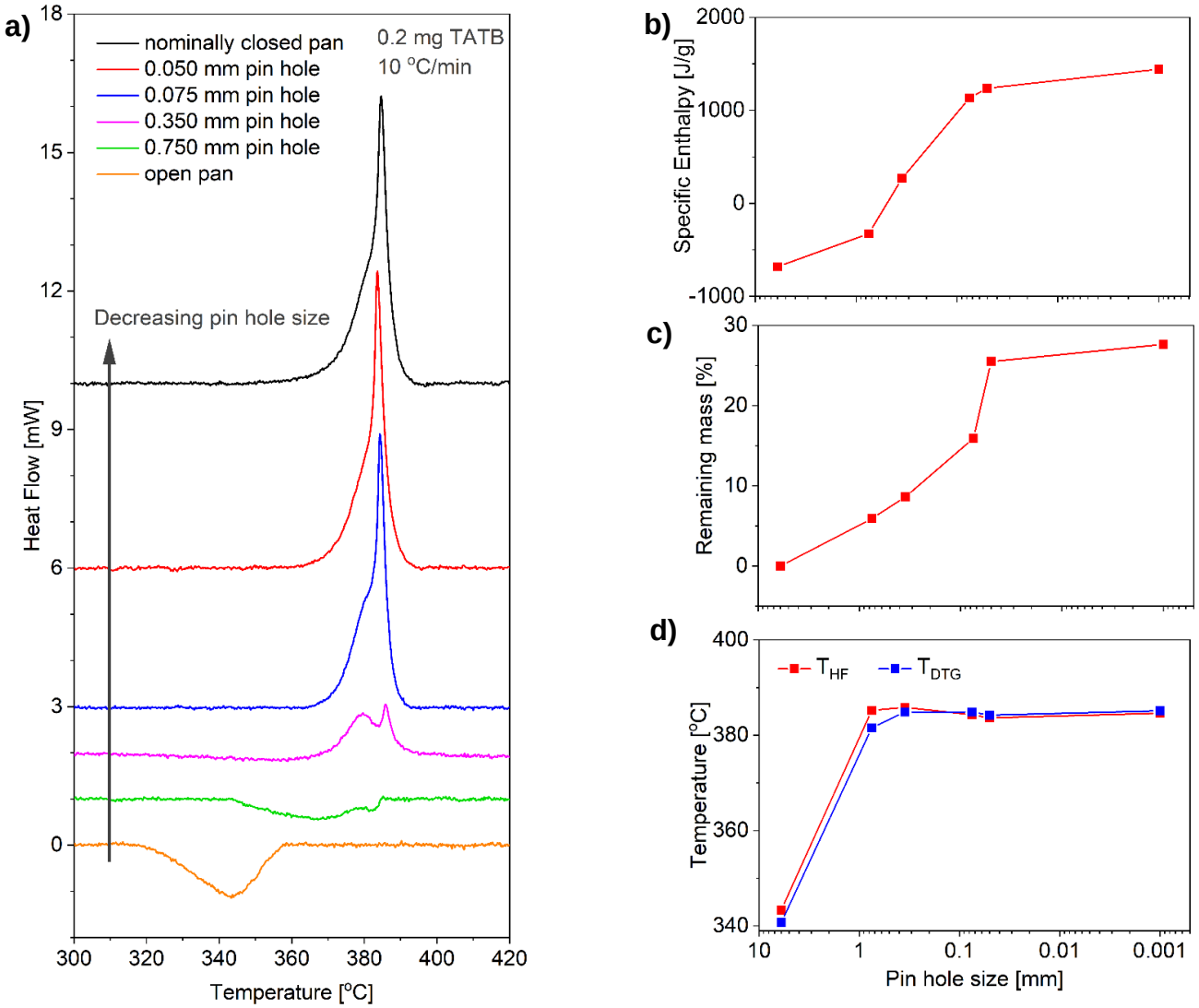

Figure 5: (a) Heat flow profiles at different pinhole sizes vs sample temperature. The data were acquired at a heating rate of 10 °C/min with nominally 0.2 mg of TATB. **(b)** Enthalpy of reaction vs pinhole size. **(c)** Amount of remaining material at the end of the tests vs pinhole size. **(d)** Temperatures from peak heat flow (T_{HF}) and peak weight loss (T_{DTG}) vs pinhole size.

3.2. Effect of Starting mass

Figure 6 (a) shows the heat flow profiles as a function of starting mass for the experiments performed with 0.075 mm pinholes at a heating rate of 10 °C/min. The starting mass was varied over a narrow range (~100 µg) from 0.120 mg to 0.222 mg. The first exotherms appeared as leading shoulders before the second exotherms for all the starting masses explored. The second exotherm became sharper as the starting mass increased. Figure 6 (b) shows that the enthalpy of reaction increased by about 600 J/g with increasing starting mass. Figure 6 (c) and (d) show the amount of remaining material and peak temperatures as a function of starting mass, respectively. The remaining mass was relatively constant except for two data points (0.182 mg and 0.194 mg) that showed slightly lower values. The specific enthalpies were also lower for the same data points, so there seems to be a correlation between the specific enthalpy and amount of remaining material. The peak temperatures showed a generally decreasing trend with increasing starting mass.

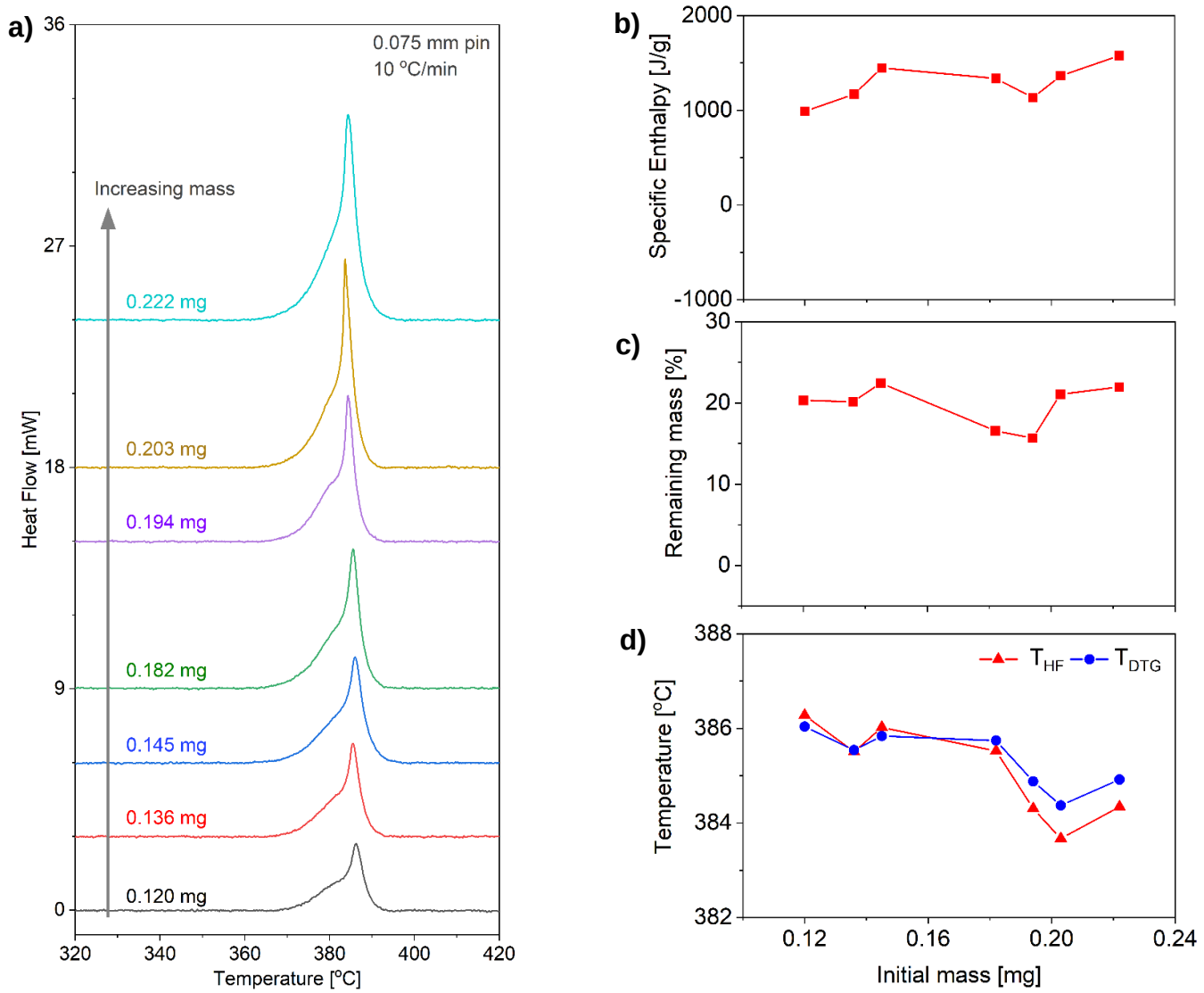

Figure 6: (a) Heat flow profiles at different starting masses vs sample temperature. The data were acquired at a heating rate of 10 °C/min with nominally 0.075 mm pinholes. **(b)** Enthalpy of reaction vs mass. **(c)** Amount of remaining material at the end of the tests vs starting mass. **(d)** Temperatures from peak heat flow (T_{HF}) and peak weight loss (T_{DTG}) vs starting mass.

Figure 7 (a) shows the DSC curves as a function of starting mass for the experiments performed with 0.075 mm pinholes at a heating rate of 5 °C/min. The range of starting mass was wider (200 µg) in this case from 0.186 mg to 0.408 mg. Two separate exotherms were observed when the starting material was small (e.g., 0.186 mg). The relative intensity of the second exotherm with respect to the first increased as the starting mass was raised from 0.186 mg to 0.314 mg. Above that mass, the resolution of the first and second exotherms varied a little with no clear trend. Figure 7 (b) shows the specific enthalpy of reaction as a function of starting mass. The overall trend in enthalpy is to increase from about 200 J/g to about 1500 J/g as mass increases from 0.186 to 0.408 mg. Simultaneously, the second exotherm becomes more prominent and tends to merge with the leading shoulder. So, there seems to be a correlation between the heat flow profiles (i.e., a transition from two peaks towards a single peak) and the enthalpy of reaction indicative of more complete reaction with larger

mass. The deviation from a smooth trend may reflect measurement precision, an effect of particle shape, or some combination thereof.

Figure 7 (c) and (d) show the amount of remaining material and peak temperatures as a function of starting mass, respectively. The remaining mass followed a very similar trend with enthalpy, i.e., the enthalpy first increased and then slightly decreased but increased back again as the starting mass increased. The difference between the two peak temperatures was around 0.6°C when the starting mass was small (e.g., 0.186 mg). However, as the starting mass increased to 0.262 mg, the difference decreased to less than 0.1°C. In addition, as the starting mass increased closer to the self-heating limit[23], the temperatures obtained from the heat-flow curves became lower than those obtained from the weight loss measurements. The peak temperatures had a generally decreasing trend with increasing starting mass.

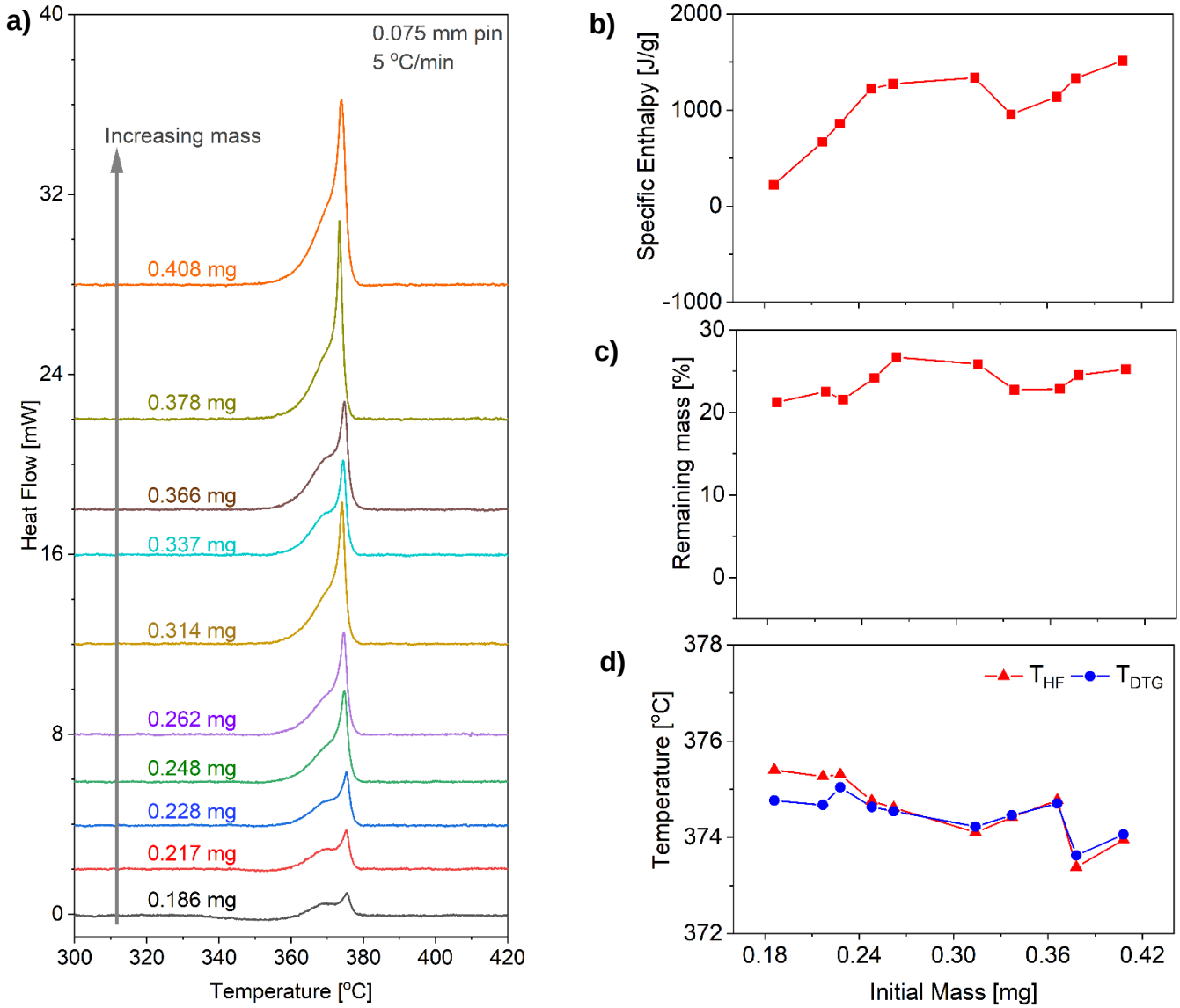

Figure 7: (a) Heat flow profiles at different starting masses vs sample temperature. The data were acquired at a heating rate of 5 °C/min with nominally 0.075 mm pinhole. **(b)** Enthalpy of reaction vs starting mass. **(c)** Amount of remaining material at the end of the tests vs starting mass. **(d)** Temperatures from peak heat flow (T_{HF}) and peak weight loss (T_{DTG}) vs starting mass.

Figure 8 (a) shows the DSC curves as a function of starting mass for the experiments performed with 0.75 mm pinholes at a heating rate of 5°C/min. The starting mass was varied in a much wider range (500 µg) from 0.259 mg to 0.774 mg. An endotherm and a barely discernable exotherm were observed for the smallest mass studied. Two exotherms having equal magnitudes were seen until the starting mass was increased to 0.485 mg. The magnitude of the second exotherm increased with respect to the first with further increase of the mass. Figure 8 (b), (c), and (d) show the enthalpy of reaction, remaining mass, and peak temperatures as a function of starting mass, respectively. The two peak temperatures (T_{HF} and T_{DTG}) were significantly different from each other (> 1.5°C) until the starting mass was raised to 0.485 mg. Further increase of the starting mass reduced the temperature difference to 0.2°C. This agrees with the results shown in Figure 5 (i.e., the temperature difference is large when there is significant sublimation). Similarly, the specific enthalpy and remaining mass increased as the starting mass was increased, which is due to sublimation being less significant at larger starting masses.

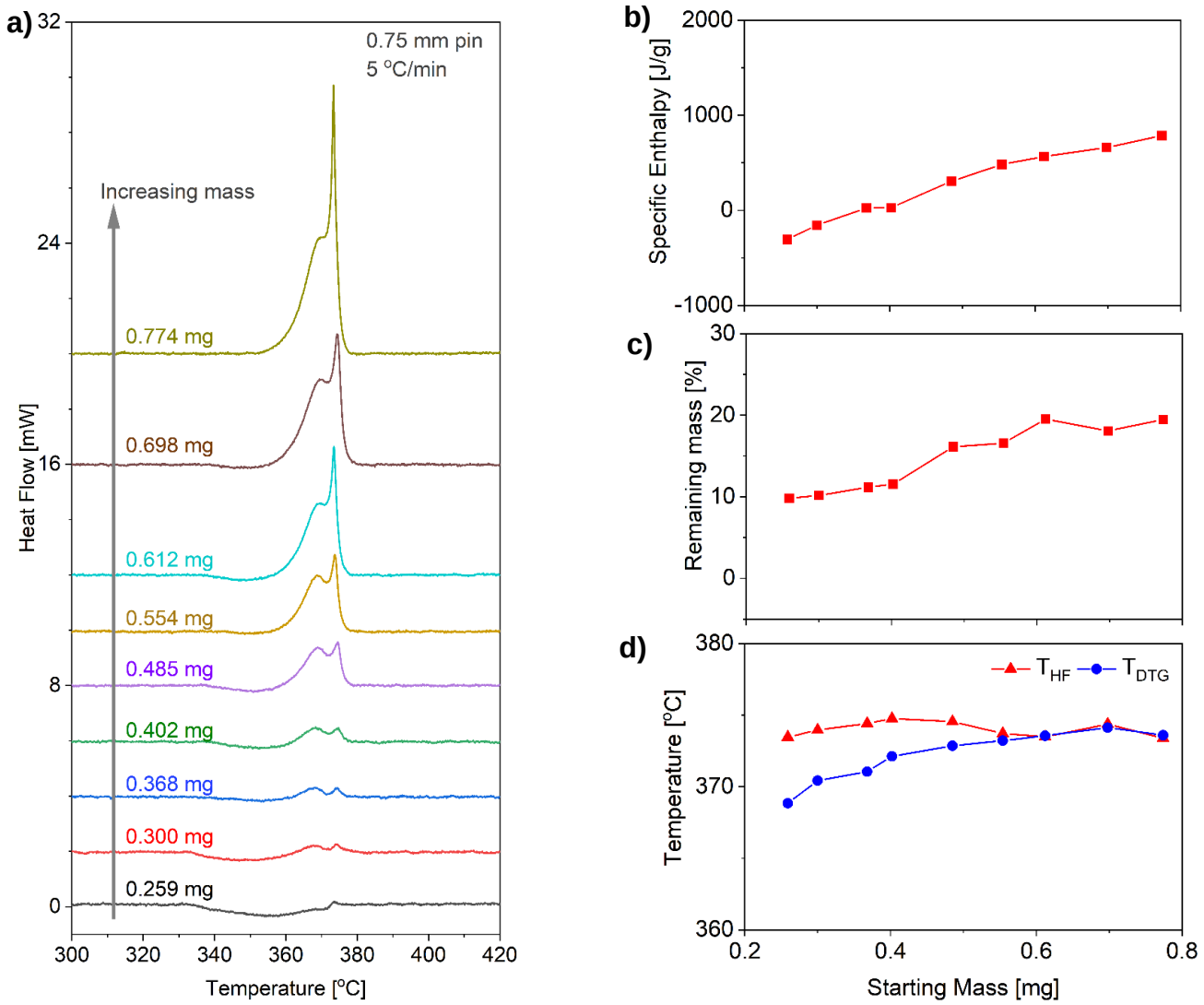

Figure 8: (a) Heat flow profiles at different starting masses vs sample temperature. The data were acquired at a heating rate of 5 °C/min with nominally 0.75 mm pinhole. **(b)** Enthalpy of reaction vs mass. **(c)** Amount of remaining material at the end of the tests vs starting mass. **(d)** Temperatures from peak heat flow (T_{HF}) and peak weight loss (T_{DTG}) vs starting mass.

To see the influence of all three variables (starting mass, heating rate, and pinhole size) on heat flow, we have plotted Figure 9, which displays the peak heat flow along the left y-axis (with filled circles) as a function of starting mass for two different heating rates (10 and 5 °C/min) and two different pinhole sizes (0.075 and 0.75 mm). For a specific pinhole size and heating rate, increasing the starting mass increases the peak heat flow in all three cases. For a 0.075 mm pinhole, increasing the heating rate from 5 to 10 °C/min increases the peak heat flow for a given starting mass. For 5 °C/min heating rate, increasing the pinhole size from 0.075 to 0.75 mm reduces the maximum heat flow due to sublimation. Figure 9 also shows the temperature differences corresponding to the peak heat flow values. The temperature difference is between the reference pan ($T_{reference}$) and sample pan (T_{sample}). The temperature differences are plotted along the right y-axis with hollow circles. The ASTM[23] limit of self-heating (HF < 8 mW) is included in the figure as a dashed horizontal line. To avoid self-heating and the resulting temperature gradients within the sample, the temperature difference between the reference and sample pans should be kept below 0.4°C for TATB, which is slightly lower than recommended earlier[2].

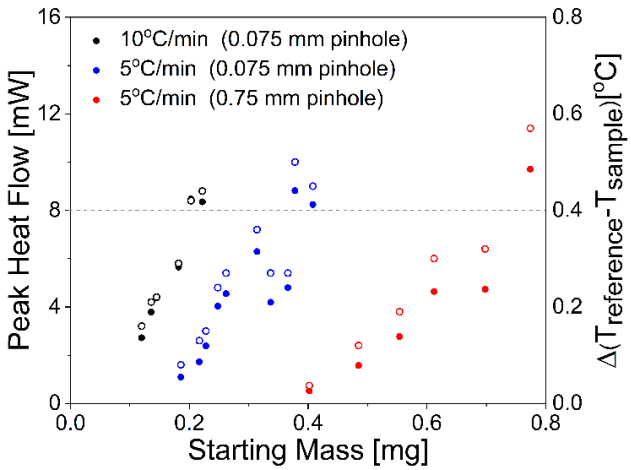

Figure 9: Peak heat flow (filled circles) and $\Delta(T_{reference}-T_{sample})$ (hollow circles) are plotted along the left and right-y axes, respectively.

4. DISCUSSION

The efflux of the volatiles from a TGA/DSC pan depends on geometric factors such as the pan volume (fixed to 40 µL in this study) and pinhole size, and the rate at which the gas-phase chemical species are produced via phase change (e.g., sublimation) and thermal decomposition. TATB sublimation is a function of temperature and if the vapor pressure of TATB reaches its saturation pressure at a given temperature inside the TGA/DSC pan, then TATB will no longer sublime. As a result, TATB will thermally decompose rather than sublime. This is the reason why Figure 5 shows an increasing trend in enthalpy and remaining mass with decreasing pinhole size for a given starting mass (0.2 mg of TATB). A transition occurs from a sublimation-dominated regime towards a decomposition-dominated regime by increasing the confinement.

Both peak temperatures (T_{HF} and T_{DTG}) also increase with decreasing pinhole size, and they also converge. When the pinhole size is small (e.g., 0.075 mm), the increase in starting mass results in smaller increases in the enthalpy of reaction and amount of remaining mass, as shown in Figures 6 and 7 for 10 °C/min and 5 °C/min, respectively. In these two cases, the results do not seem to be dictated by TATB sublimation. There could be an enhancement in autocatalytic reactions with increasing starting mass in a well-confined TGA/DSC pan due to an increase in the containment of gas-phase species. The decreases in peak temperatures shown in Figures 6 and 7 also support this argument. Furthermore, Figures 6 and 7 show some data points with slight decreases in enthalpies and remaining masses with increasing starting masses. These data points show corresponding changes in heat flow profiles (e.g., a transition back to a single exotherm from two exotherms). A detailed model of the diffusion/advection process out of the TGA/DSC pan could be a future study to explain this behavior. For example, the decrease in sublimation at certain starting masses might first increase the amount of thermal decomposition products inside the pan, and as a result, raise the partial pressure inside the pan. This could change the dynamics of the diffusion/advection process out of the pan and influence the sublimation process. As a result, sublimation might become relevant again for a certain regime of starting masses.

The results shown in Figure 8 seem to exhibit both behaviors discussed above: a transition from a sublimation dominated regime and an enhancement in autocatalytic reactions. This could be due to the use of a large pinhole (0.75 mm) and a larger range of starting mass (500 µg). For starting masses smaller than 0.5 mg, the two peak temperatures are quite different from each other. They both increase with increasing starting mass and then converge. This resembles the behavior displayed in Figure 5. Therefore, this should be the sublimation dominated regime. Increasing the starting mass past 0.5 mg somewhat increases the enthalpy and remaining mass, and there is a slight decrease in peak temperature corresponding to the maximum heat flow. In this regime, the two peak temperatures follow a similar trend with increasing mass. These behaviors look very similar to those depicted in Figures 6 and 7.

The DSC technique has been applied to TATB in previous publications[28–31,34–37]. The results have been widely varied, particularly in the relationship of the two exotherms, whether the first is a leading edge shoulder or a distinct exotherm. In this study, this variability is observed with changes in pinhole size as shown in Figure 5 (due to the competition between sublimation and decomposition), as well as with changes in sample size as shown in Figures 7 and 8 (potentially due to the added effect of enhanced autocatalysis with increasing starting mass). A major finding of this study is the real need for control of variables affecting instrumental output — sample size, pinhole size, and heating rate. Until precise control of the conditions is manifested, comparison of other process properties (e.g., TATB synthesis method[37,38], solvents used for TATB purification[39–44]) will not be possible to achieve, and the utility of using DSC for safety evaluations will be greatly diminished.

5. CONCLUSIONS

The influence of three variables (confinement, starting mass, and heating rate) on TATB sublimation and thermal decomposition were investigated using a combined Thermo-Gravimetric Analyzer and Differential Scanning Calorimetry (TGA/DSC) setup. The measurements were performed at atmospheric pressure. The range of experimental variables were chosen such that the maximum heat flow signal did not exceed 8 mW and therefore the self-heating of the samples was minimized. This study showed self-heating of the samples was not only a function of starting mass and heating rate, but it also depended on the degree of confinement. The confinement of volatiles inside the TGA/DSC pans was varied by changing the pinhole sizes of the lids. Six different orifice sizes were tested. The influence of starting mass was studied using two different pinhole sizes (0.075 and 0.75 mm) and two different heating rates (10 and 5 °C/min).

The measurements performed as a function of pinhole size showed a strong competition between the rate of TATB sublimation and TATB thermal decomposition. As the pinhole size was decreased for a given starting mass and heating rate, the enthalpy of reaction increased. Similarly, the amount of remaining material and the peak temperatures corresponding to maximum heat flow and weight loss increased as well. The difference between the two peak temperatures (T_{HF} and T_{DTG}) decreased from 4 °C to 0.6 °C. In addition, a transition from two exotherms towards a single exotherm occurred with decreasing pinhole size. The enthalpy calculated from the open pan test result allowed us to determine the heat of TATB sublimation, 681 J/g (42 kcal/mol). The highest value of enthalpy was determined to be 1578 J/g (97.3 kcal/mol), and it was measured using a 0.075 mm pinhole at a heating rate of 10 °C/min with 0.222 mg of TATB. In a future study, sealed

pans that can withstand high pressures could be used to obtain the upper limit of the thermal decomposition enthalpy of TATB.

The measurements performed as a function of starting mass using a large pinhole (0.75 mm) indicated a similar transition from a sublimation dominated regime towards a thermal decomposition dominated regime. The increase in starting mass increased the enthalpy, amount of remaining material, and peak temperatures. When an order of magnitude smaller pinhole was used (0.075 mm), sublimation was suppressed substantially and increasing the starting mass resulted in slight increases in enthalpy and remaining mass. Interestingly, the peak temperatures showed a generally decreasing trend with increasing starting mass. This could be due to the enhancement of autocatalytic reactions with an increase in the containment of gas-phase species. Also, a clear correlation was observed in heat flow profiles such that a transition from two exotherms towards a single exotherm always resulted in an increase in the enthalpy of reaction and amount of remaining material.

ACKNOWLEDGMENTS

This work was performed under the auspices of the U.S. Department of Energy by Lawrence Livermore National Laboratory under Contract DE-AC52-07NA27344. We are thankful to Franco Gagliardi for pressing the HE samples. We are also thankful to Jason Moore, Keith Coffee, Keith Morrison, John Rosener, Jennifer L. Montgomery, Greg Klunder, and Matt McCleland for their insightful discussions.

5. REFERENCES

(1) Koroglu, B.; Crowhurst, J. C.; Kahl, E. M.; Moore, J. S.; Racoveanu, A.; Mason, H. E.; Weisz, D. G.; Reynolds, J. G.; Burnham, A. K. Experimental Investigation of the Thermal Decomposition Pathways and Kinetics of TATB by Isotopic Substitution. *Propellants Explos. Pyrotech.* **2021**, *46* (9), 1352–1366. https://doi.org/10.1002/prep.202100082.

(2) Burnham, A. K.; Stanford, V. L.; Vyazovkin, S.; Kahl, E. M. Effect of Pressure on TATB and LX-17 Thermal Decomposition. *Thermochim. Acta* **2021**, 178908. https://doi.org/10.1016/j.tca.2021.178908.

(3) Wemhoff, A. P.; Becker, R.; Burnham, A. K. Calibration of Chemical Kinetic Models Using Simulations of Small-Scale Cookoff Experiments. In *HT2008*; Heat Transfer: Volume 3, 2008; pp 93–101. https://doi.org/10.1115/HT2008-56108.

(4) Suşeska, M.; Rajiş, M.; Matečiş-Mušaniş, S.; Zeman, S.; Jalový, Z. Kinetics and Heats of Sublimation and Evaporation of 1,3,3-Trinitroazetidine (TNAZ). *J. Therm. Anal. Calorim.* **2003**, *74* (3), 853–866. https://doi.org/10.1023/B:JTAN.0000011017.65451.96.

(5) Vyazovkin, S.; Wight, C. A. Kinetics of Thermal Decomposition of Cubic Ammonium Perchlorate. *Chem. Mater.* **1999**, *11* (11), 3386–3393. https://doi.org/10.1021/cm9904382.

(6) Gorn, M. V.; Monogarov, K. A.; Dalinger, I. L.; Melnikov, I. N.; Kiselev, V. G.; Muravyev, N. V. Pressure DSC for Energetic Materials. Part 2. Switching between Evaporation and Thermal Decomposition of 3,5-Dinitropyrazole. *Thermochim. Acta* **2020**, *690*, 178697. https://doi.org/10.1016/j.tca.2020.178697.

(7) Behrens, R. *Thermal Decomposition of Energetic Materials: TNCHP, TNAZ, 24DNI, ANTA, DNBT AND HMX*; ARO 33655.2-CH; SANDIA NATIONAL LABS LIVERMORE CA COMBUSTION RESEARCH FACILITY, 1998.

(8) Farber, M.; Srivastava, R. D. Thermal Decomposition of 1,3,5-Triamino-2,4,6-Trinitrobenzene. *Combust. Flame* **1981**, *42*, 165–171. https://doi.org/10.1016/0010-2180(81)90155-3.

(9) Singh, A.; Sharma, T. C.; Kishore, P. Thermal Degradation Kinetics and Reaction Models of 1,3,5-Triamino-2,4,6-Trinitrobenzene-Based Plastic-Bonded Explosives Containing Fluoropolymer Matrices. *J. Therm. Anal. Calorim.* **2017**, *129* (3), 1403–1414. https://doi.org/10.1007/s10973-017-6335-z.

(10) Belmas, R.; Bry, A.; David, C.; Gautier, L.; Keromnès, A.; Poullain, D.; Thevenot, G.; Gallic, C. L.; Chenault, J.; Guillaumet, G. Preheating Sensitization of a TATB Composition Part One: Chemical Evolution. *Propellants Explos. Pyrotech.* **2004**, *29* (5), 282–286. https://doi.org/10.1002/prep.200400059.

(11) Makashir, P. S.; Kurian, E. M. Spectroscopic and Thermal Studies on the Decomposition of l,3,5-Triamino-2,4,6-Trinitrobenzene (TATB). *J. Therm. Anal.* **1996**, *46* (1), 225–236. https://doi.org/10.1007/BF01979963.

(12) Brill, T. B.; James, K. J. Thermal Decomposition of Energetic Materials. 61. Perfidy in the Amino-2,4,6-Trinitrobenzene Series of Explosives. *J. Phys. Chem.* **1993**, *97* (34), 8752–8758. https://doi.org/10.1021/j100136a017.

(13) Bulusu, S.; Behrens, R., Jr. The Importance of Mononitroso Analogues of Cyclic Nitramines to the Assessment of the Safety of HMX-Based Propellants and Explosives, International Journal of Energetic Materials and Chemical Propulsion, 1997, *4*, 278–289.

(14) Bulusu, S.; Behrens, R., Jr. A Review of. the Thermal Decomposition Pathways in RDX, HMX and Other Closely Related Cyclic Nitramines. *Def. Sci. J.* 1996, *46* (5), 347.

(15) Behrens, R., Jr.; Wiese-Smith, D.; Johnston, L. A.; Maharrey, S. P. *Evaluation of Ingredients for the Development of New Insensitive Munitions.*; United States, 2004. https://doi.org/10.2172/920116.

(16) Hayden, H. F. Thermal Decomposition of High-Nitrogen Energetic Compounds: TAGzT and GUzT. Ph.D., The George Washington University, United States -- District of Columbia, 2009.

http://library-r-ez.llnl.gov:2048/dissertations-theses/thermal-decomposition-high-nitrogen-energetic/docview/89125174/se-2?accountid=12131.
(17) Mozaffari, P.; Järvik, O.; Baird, Z. S. Vapor Pressures of Phenolic Compounds Found in Pyrolysis Oil. *J. Chem. Eng. Data* **2020**, *65* (11), 5559–5566. https://doi.org/10.1021/acs.jced.0c00675.
(18) Butrow, A. B.; Seyler, R. J. Vapor Pressure by DSC: Extending ASTM E 1782 below 5 KPa. *Thermochim. Acta* **2003**, *402* (1), 145–152. https://doi.org/10.1016/S0040-6031(02)00604-4.
(19) Brozena, A. Vapor Pressure of 1-Octanol below 5kPa Using DSC. *Thermochim. Acta* **2013**, *561*, 72–76. https://doi.org/10.1016/j.tca.2013.03.018.
(20) Contreras, M. D.; Girela, F.; Parera, A. The Perfection of a Method for the Determination of the Temperature/Vapour-Pressure Function of Liquids by Differential Scanning Calorimetry. *Thermochim. Acta* **1993**, *219*, 167–172. https://doi.org/10.1016/0040-6031(93)80494-U.
(21) Perrenot, B.; de Vallière, P.; Widmann, G. New Pressure DSC Cell and Some Applications. *J. Therm. Anal.* **1992**, *38* (3), 381–390. https://doi.org/10.1007/BF01915502.
(22) Siitsman, C.; Oja, V. Extension of the DSC Method to Measuring Vapor Pressures of Narrow Boiling Range Oil Cuts. *Appl. Therm. Anal. Tech. Sublimation Vap. Stud.* **2015**, *622*, 31–37. https://doi.org/10.1016/j.tca.2015.04.011.
(23) *ASTM E537-20 Standard Test Method for The Thermal Stability of Chemicals by Differential Scanning Calorimetry*; 2020.
(24) *Thermal Analysis Application Handbook Evolved Gas Analysis*; No. HB 600; Mettler Toledo, 2019.
(25) Schubnell, M.; Regonini, D. *Mettler Toledo Thermal Analysis Information for Users - User Com 53*; page 6, Table 2; 2021.
(26) Coffee, K. R.; Panasci-Nott, A. F.; Stewart, B. J.; Olivas, J. A.; Williams, A. M.; Reynolds, J. G. Trace Compound Analysis in TATB by Liquid Chromatography Coupled with Spectroscopic and Spectrometric Detection. *Propellants Explos. Pyrotech.* **2022**, *47* (4), e202100224. https://doi.org/10.1002/prep.202100224.
(27) W. Rasband, "ImageJ," Https://Imagej.Nih.Gov. (1997–2018).
(28) Catalano, E.; Crawford, P. C. An Enthalpic Study of the Thermal Decomposition of Unconfined Triaminotrinitrobenzene. *Thermochim. Acta* **1983**, *61* (1), 23–36. https://doi.org/10.1016/0040-6031(83)80301-3.
(29) Zeman, S. The Thermoanalytical Study of Some Aminoderivatives of 1,3,5-Trinitrobenzene. *Thermochim. Acta* **1993**, *216*, 157–168. https://doi.org/10.1016/0040-6031(93)80389-R.
(30) Singh, A.; Sharma, T. C.; Kumar, M.; Narang, J. K.; Kishore, P.; Srivastava, A. Thermal Decomposition and Kinetics of Plastic Bonded Explosives Based on Mixture of HMX and TATB with Polymer Matrices. *Def. Technol.* **2017**, *13* (1), 22–32. https://doi.org/10.1016/j.dt.2016.11.005.
(31) Glascoe, E. A.; Maienschein, J. L.; Lorenz, K. T.; Tan, N.; Koerner, J. G. Deflagration Rate Measurements of Three Insensitive High Explosives: LLM-105, TATB, and DAAF. In *14th International Detonation Symposium Coeur D'Alene, ID, United States, LLNL-PROC-425285*; 2010.
(32) Rosen, J. M.; Dickinson, C. Vapor Pressures and Heats of Sublimation of Some High-Melting Organic Explosives. *J. Chem. Eng. Data* **1969**, *14* (1), 120–124. https://doi.org/10.1021/je60040a044.
(33) Garza, R. G. *Thermogravimetric Study of TATB and Two TATB-Based Explosives*; UCRL-82723; California Univ., Livermore (USA). Lawrence Livermore Lab., 1979.
(34) Schaffer, C. L. *Recrystallization of TATB for Analytical Standard*; United States, 1980. https://doi.org/10.2172/5736258.
(35) Mark Hoffman, D.; Willey, T. M.; Mitchell, A. R.; Depiero, S. C. Comparison of New and Legacy TATBs. *J. Energ. Mater.* **2008**, *26* (3), 139–162. https://doi.org/10.1080/07370650801922195.
(36) Lewis, D.; Padfield, J.; Connors, S.; Wilson, I.; Akhavan, J. Further Insights into the Discoloration of TATB under Ionizing Radiation. *J. Energ. Mater.* **2020**, *38* (3), 362–376. https://doi.org/10.1080/07370652.2020.1716109.
(37) Bellamy, A. J.; Ward, S. J.; Golding, P. A New Synthetic Route to 1,3,5-Triamino-2,4,6-Trinitrobenzene (TATB). *Propellants Explos. Pyrotech.* **2002**, *27* (2), 49–58. https://doi.org/10.1002/1521-4087(200204)27:2<49::AID-PREP49>3.0.CO;2-4.
(38) Benziger, T. M. Method for the Production of High-Purity Triaminotrinitrobenzene, US Patent, 4032377, Energy Research and Development Administration, June 28, 1977. https://www.osti.gov/biblio/7077664.
(39) Foltz, M. F.; Ornellas, D. L.; Pagoria, P. F.; Mitchell, A. R. Recrystallization and Solubility of 1,3,5-Triamino-2,4,6-Trinitrobenzene in Dimethyl Sulfoxide. *J. Mater. Sci.* **1996**, *31* (7), 1893–1901. https://doi.org/10.1007/BF00372205.
(40) Foltz, M. F.; Maienschein, J. L.; Green, L. G. Particle Size Control of 1,3,5-Triamino-2,4,6-Trinitrobenzene by Recrystallization from DMSO. *J. Mater. Sci.* **1996**, *31* (7), 1741–1750. https://doi.org/10.1007/BF00372187.
(41) Yang, G.; Nie, F.; Huang, H.; Zhao, L.; Pang, W. Preparation and Characterization of Nano-TATB Explosive. *Propellants Explos. Pyrotech.* **2006**, *31* (5), 390–394. https://doi.org/10.1002/prep.200600053.
(42) Talawar, M. B.; Agarwal, A. P.; Anniyappan, M.; Gore, G. M.; Asthana, S. N.; Venugopalan, S. Method for Preparation of Fine TATB (2–5μm) and Its Evaluation in Plastic Bonded Explosive (PBX) Formulations. *J. Hazard. Mater.* **2006**, *137* (3),

1848–1852. https://doi.org/10.1016/j.jhazmat.2006.05.031.
(43) Nandi, A. K.; Kasar, S. M.; Thanigaivelan, U.; Ghosh, M.; Mandal, A. K.; Bhattacharyya, S. C. Synthesis and Characterization of Ultrafine TATB. *J. Energ. Mater.* **2007**, *25* (4), 213–231. https://doi.org/10.1080/07370650701567066.
(44) Han, T. Y.-J.; Pagoria, P. F.; Gash, A. E.; Maiti, A.; Orme, C. A.; Mitchell, A. R.; Fried, L. E. The Solubility and Recrystallization of 1,3,5-Triamino-2,4,6-Trinitrobenzene in a 3-Ethyl-1-Methylimidazolium Acetate–DMSO Co-Solvent System. *New J. Chem.* **2009**, *33* (1), 50–56. https://doi.org/10.1039/B810109D.